SCIENTIFIC REPORTS

OPEN

SUBJECT AREAS:
BATTERIES
CHEMICAL BIOLOGY

Received
14 September 2014

Accepted
10 December 2014

Published
13 January 2015

Correspondence and requests for materials should be addressed to S.M. (sagar.mitra@iitb.ac.in)

Flagellar filament bio-templated inorganic oxide materials – towards an efficient lithium battery anode

Sergei N. Beznosov[1], Pavan S. Veluri[2], Mikhail G. Pyatibratov[1], Abhijit Chatterjee[3], Douglas R. MacFarlane[4], Oleg V. Fedorov[1] & Sagar Mitra[2]

[1]Institute of Protein Research, Russian Academy of Sciences, 142290 Pushchino, Russia, [2]Department of Energy Science and Engineering, Indian Institute of Technology Bombay, Powai 400076 Mumbai, India, [3]Department of Chemical Engineering, Indian Institute of Technology Bombay, Powai, 400076 Mumbai, India, [4]Australian Center of Excellence for Electromaterials Science, School of Chemistry, Monash University, Clayton, Victoria 3800, Australia.

Designing a new generation of energy-intensive and sustainable electrode materials for batteries to power a variety of applications is an imperative task. The use of biomaterials as a nanosized structural template for these materials has the potential to produce hitherto unachievable structures. In this report, we have used genetically modified flagellar filaments of the extremely halophilic archaea species *Halobacterium salinarum* to synthesize nanostructured iron oxide composites for use as a lithium-ion battery anode. The electrode demonstrated a superior electrochemical performance compared to existing literature results, with good capacity retention of 1032 mAh g^{-1} after 50 cycles and with high rate capability, delivering 770 mAh g^{-1} at 5 A g^{-1} (~5 C) discharge rate. This unique flagellar filament based template has the potential to provide access to other highly structured advanced energy materials in the future.

Breakthroughs in high energy and power density lithium battery technology are strongly reliant on the development of new nanostructured electrode materials[1,2]. A new and promising trend in the creation of such materials is the use of bio-polymers for the directional assembly of inorganic components into structures of greater hierarchical complexity[3,4]. This approach was first demonstrated by Belcher and co-workers to create lithium-ion battery electrode materials based on a genetically modified, filamentous M13 virus as a bio-template[5–7]. In the present work, we demonstrate the use of *flagella* as promising, and much more easily handled, bio-templates for materials synthesis.

The standard capacity of a graphite anode in commercial batteries is only 250–300 mAh g^{-1} with the theoretical limit of 372 mAh g^{-1} [8]. Moreover, the rate performance of graphite is still well below the levels demanded for high power lithium ion batteries in advanced applications such as electric vehicles. Oxides of transition metals (such as Co, Fe, Ni, Cu, *etc.*) have attracted great attention in this regard because of their potential to deliver high theoretical specific capacity[9]. Among the metal oxides, iron oxide (Fe_2O_3) is one of the most promising materials because of its high theoretical specific capacity (1007 mAh g^{-1}), abundance, low cost and environmental acceptability[1,9,10]. At present, the fabrication and performance (in terms of cycle stability) of Fe_2O_3 based anodes still remains a great challenge[10]. It is known that under discharge/charge cycling Fe_2O_3 based electrode materials degrade and their capacity fades quickly[11]. In addition, the active surface area of such materials reduces because of agglomeration[12,13]. One of the ways to overcome these imperfections is to fabricate hybrid nanostructures, where Fe_2O_3 is embedded into a conductive matrix or covered with coating layers via intermolecular interactions or to synthesize nanostructured Fe_2O_3 or nanoparticles, nanowires *etc.*[13–18].

Viruses and other biological structures that can function as scaffolds can stabilize such nanosized metal oxide particles and prevent their agglomeration[5,6]. Bacterial and archaeal *flagella* are structures that have attractive properties for this use[19–23]. These are extracellular protein filaments used by unicells as motility organelles. The Archaea constitute a domain of microorganisms mostly composed of cells that live in extreme environments. Many archaeal biopolymers, including flagella, are able to preserve their structural integrity in a wide range of external conditions. As such they may be promising candidates as synthetic templates in nanobiotechnology[24]. Archaeal flagella are typically long (~10 μm) filaments with thickness of 10–15 nm[25]. Being totally protein-based structures, they offer a number of benefits over DNA-containing viruses in nano-technology applications. Halophilic archaea are safe to humans and quite un-demanding in terms of growth environment (advanta-

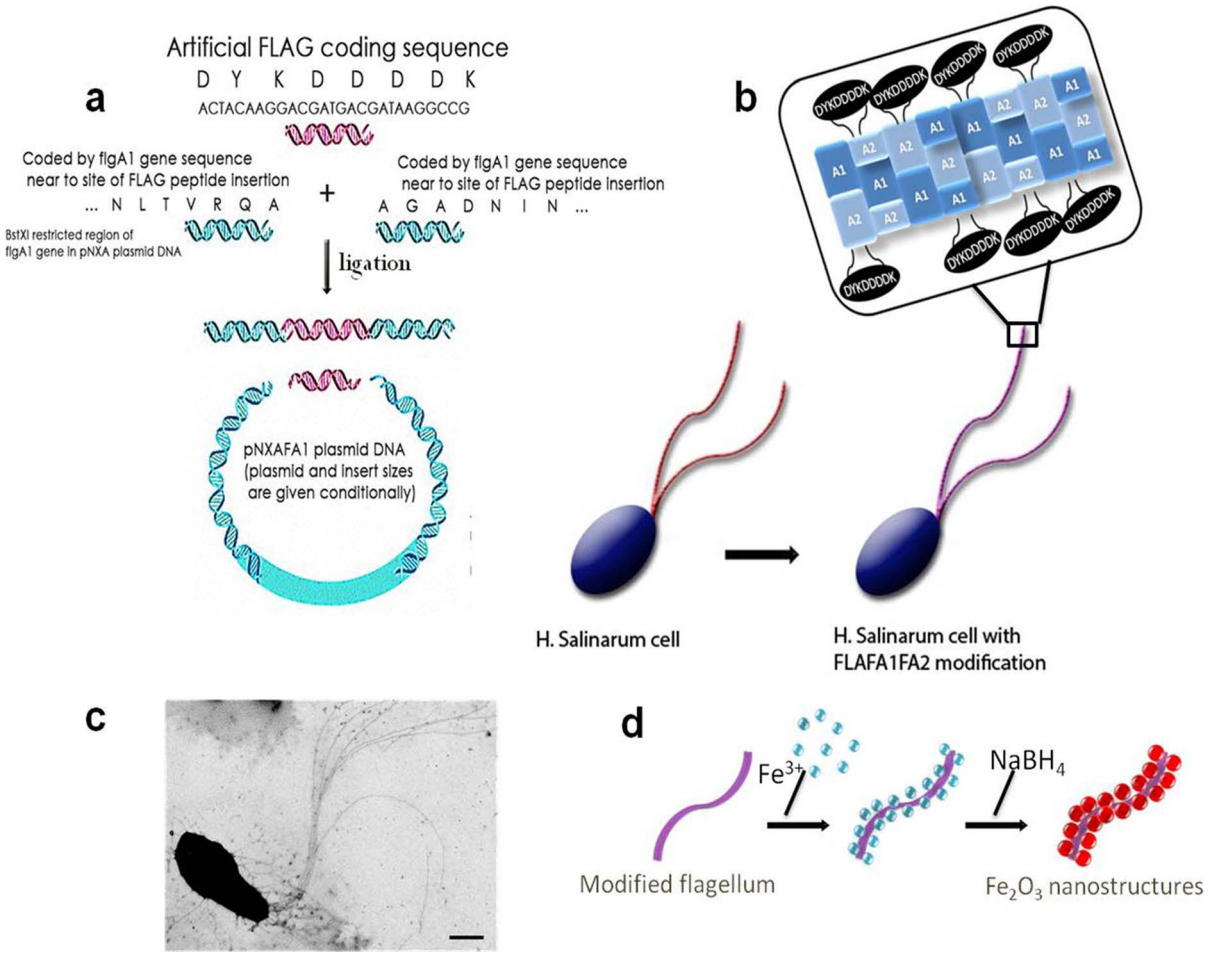

Figure 1 | Schematic of the gene modification and mineralization (a) FLAG peptide insertion at Flg*A1* gene site, (b) *H. salinarum* cell after modifications at both FlgA1 and FlgA2 genes (inset shows coding sequence), (c) TEM image of the flagellated *H. salinarum* cell (scale bar is 300 nm) and (d) Incubation of modified flagellum in aqueous Fe^{3+} solution and its conversion to Fe_2O_3.

geously, requiring a high salt concentration), and modified flagella can be isolated and purified easily with yields up to 20 mg L^{-1} (compared to 10 mg L^{-1} in the case of M13 viruses). Previously, we have demonstrated the use of flagella of halophilic archaea species *Halobacterium salinarum* as a biotemplate for the selective binding of target substances[21,26]. *H. salinarum* flagellar filaments are formed from five homologous protein subunits-flagellins FlgA1, A2, B1, B2, B3 in which FlgA1 and A2 are the major components which are distributed along the full filament length[26,27]. To create binding sites for templating purposes, genetically modified strains can be constructed[21,26] such that FlgA1 and A2 are modified with an inserted FLAG peptide (DYKDDDDK) sequence[21,26]. The carboxyl groups of aspartate and glutamate side chains are good sites for positively charged ion binding. The aspartate rich FLAG peptide was designed as a tag which was introduced into the target proteins for their subsequent purification by immunoaffinity chromatography and could be conveniently detected by commercial antibodies[28]. The FLAG peptide insertion does not affect the flagellum assembly and creates metal cation binding sites on the exposed surfaces of the flagella. These sites can then become nucleation points for the growth of inorganic oxide nanoparticles.

In the current study, we have synthesized Fe_2O_3 nanostructured anode materials using *H. salinarum* flagella as a bio-template. Multi-walled carbon nanotubes (MWCNTs) were composited with these materials to improve their electronic conductivity in lithium storage applications. The effect of flagella modifications (with different peptides) and MWCNTs loading on the electrochemical performance has been investigated. Three types of modified *H. salinarum* flagella were used in this report: FA1FA2 flagella where both FlgA1 and A2 flagellins were modified by the FLAG (DYKDDDDK) peptide, FA1 flagella with FLAG peptide modified FlgA1 and EA1EA2 flagella with both FlgA1 and A2 subunits modified with the DYKEEEEK peptide (this is similar to FLAG but with 4 tandem aspartates replaced by glutamates). As already mentioned, these inserts do not lead to critical changes in the spatial structure of flagellin, which retain the ability to assemble a functional flagellum. The purpose of the peptide modifications is to provide sites that help in binding the metal cations (Fe^{3+}) to the flagella. Details of the peptide insertion procedure, a modified flagella isolation procedure and the flagella templated Fe_2O_3 nanostructured material synthesis are summarized in Fig. 1 and in the supplementary information (Fig. S1). It should be mentioned that in Belcher's experiments the tetra-glutamate peptide was used to amplify metal ion binding properties of the M13 virus[5]. The aspartate side chain is shorter than in glutamate and is less flexible, possessing one less torsion angle. Nevertheless, glutamate and aspartate do not significantly differ in their ability to bind metal ions. So, poly-L-aspartic acid and poly-L-glutamic acid immobilized onto pore glass, demonstrated similar binding strengths for the metal ions studied[29]. However, in the context of the surrounding amino acid residues this may not be the case. From the secondary structure prediction using PSIPRED[30], the spatial organizations of tetra-aspartate inserted into both A1 and A2 flagellin differ significantly from that of the glutamate analogues (Fig. S2). Taking disordered conformations the aspartates have increased availability for binding

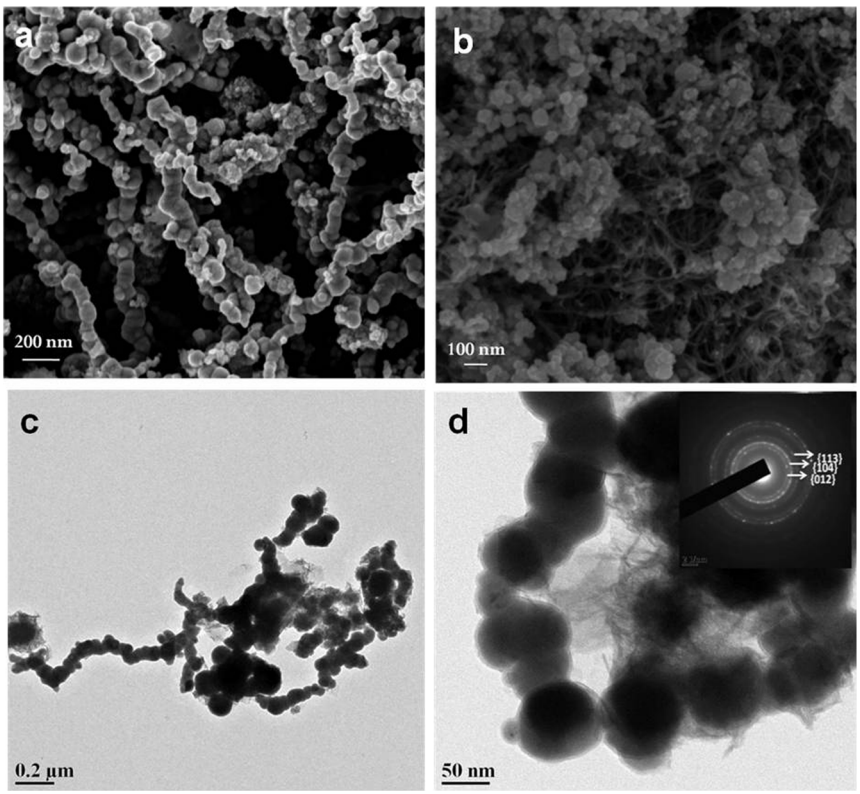

Figure 2 | Electron microscope images of mineralized samples (a), (b) FE-SEM images of FA1FA2 mineralized Fe_2O_3 sample without and with 10% MWCNTs, respectively and (c), (d) TEM images of FA1FA2 mineralized Fe_2O_3 sample [inset of (d) shows SAED pattern of FA1FA2-Fe_2O_3].

iron ions. In contrast, the glutamates, part of an alpha helix or beta strand, may be less accessible to external ions. In addition, these secondary structure elements tend to interact with other regions of the polypeptide chain, which may lead to additional stabilization of the filament structure.

Electron microscopy studies on the flagella based samples mineralized with Fe_2O_3 reveal chain like morphologies that replicate the morphology of individual flagella. FE-SEM analysis depicts uniform growth of Fe_2O_3 on the surface of FA1FA2 modified flagella (Fig. 2a). Interconnectivity of the metal oxide nanoparticles grown on the biotemplate is revealed by TEM analysis and the SAED pattern represents the {012}, {104} and {113} crystal planes of α-Fe_2O_3 (Fig. 2c, d). FE-SEM and TEM images of FA1 and EA1EA2 modified Fe_2O_3 samples are shown in Fig. S3 for comparison. Figure 2b show FE-SEM image of FA1FA2 modified samples with 10 weight % MWCNTs loading. It is clearly seen that the MWCNTs are homogeneously distributed throughout the FA1FA2-Fe_2O_3 samples, creating a percolating network for excellent electrical conductivity during the electrochemical conversion reaction with Lithium.

Figure 3a shows the charge-discharge profiles of the negative electrode materials prepared using FA1, FA1FA2 and EA1EA2 modified flagella mineralized with Fe_2O_3. The nature of the discharge profile suggests that there is no significant conversion reaction of Fe_2O_3 occurring with Lithium (Fig. 3a, b). It was demonstrated previously that biological structures based on the M13 virus are electrochemically inactive in the applied potential window[5], and it was further observed by Tarascon's group that their presence deteriorates the electrochemical reactivity of oxides towards Lithium[31]. In fact, these biological templates act as a nonconductive additive that can destroy electron and ion percolation networks[31].

It is well known that the ohmic resistance and the charge transfer resistance of the electrode formed by iron oxides are quite high. Even though we have added a conductive carbon additive it was not sufficient to form a proper percolating network to connect the nanoparticles. To achieve a better percolation network with such nanosized active materials, it is necessary to have some fraction of high aspect ratio,conductive additive that can maintain the electrical contacts between active materials during cycling. In the absence of such an additive, parts of the electrode can experience lower (more negative) voltages than others, thereby encouraging electrolyte breakdown and SEI formation reactions which eventually during cycling render these regions inactive.

In the current work, to improve the electrochemical performance, a composite material has been prepared by introducing MWCNTs into the mineralized flagella materials. Figure 3c shows the charge-discharge profiles of materials composed of flagella mineralized by Fe_2O_3 with 10 weight % MWCNTs loading for three different gene modifications (FA1, FA1FA2 and EA1EA2). After adding MWCNTs, the charge consumed in the electrochemical conversion reaction is enhanced and a well-established plateau is observed (~0.8 V *vs.* Li). Reversible charge capacity of 940 mAh g^{-1}, 1300 mAh g^{-1} and 1145 mAh g^{-1} were observed at 50 mA g^{-1} (50 mA g^{-1} = approximately a C / 20 rate, 1C = 1007 mA g^{-1}) for FA1, FA1FA2 and EA1EA2 gene modifications, respectively. The latter two of these results are higher than theoretical capacity for pure Fe_2O_3 (1007 mAh g^{-1}), suggesting that some additional charging mechanism, perhaps a pseudo-capacitive contribution and lithium intercalation in MWCNTs together, is part of this overall capacity.

To test electrochemical stability, the first three cycles were tested at 50 mA g^{-1} and the remaining cycles were tested at the much higher current rate of 593 mA g^{-1} (~C / 2). Capacity fading was observed in the case of EA1EA2 and FA1 samples, but rather stable capacity was achieved with FA1FA2 samples (Fig. 3d). After 50 cycles, 1032 mAh g^{-1} capacity was still retained in the case of FA1FA2 samples at the 593 mA g^{-1} rate. The enhancement in electronic conductivity in the presence of MWCNTs is responsible for the stable electrochemical

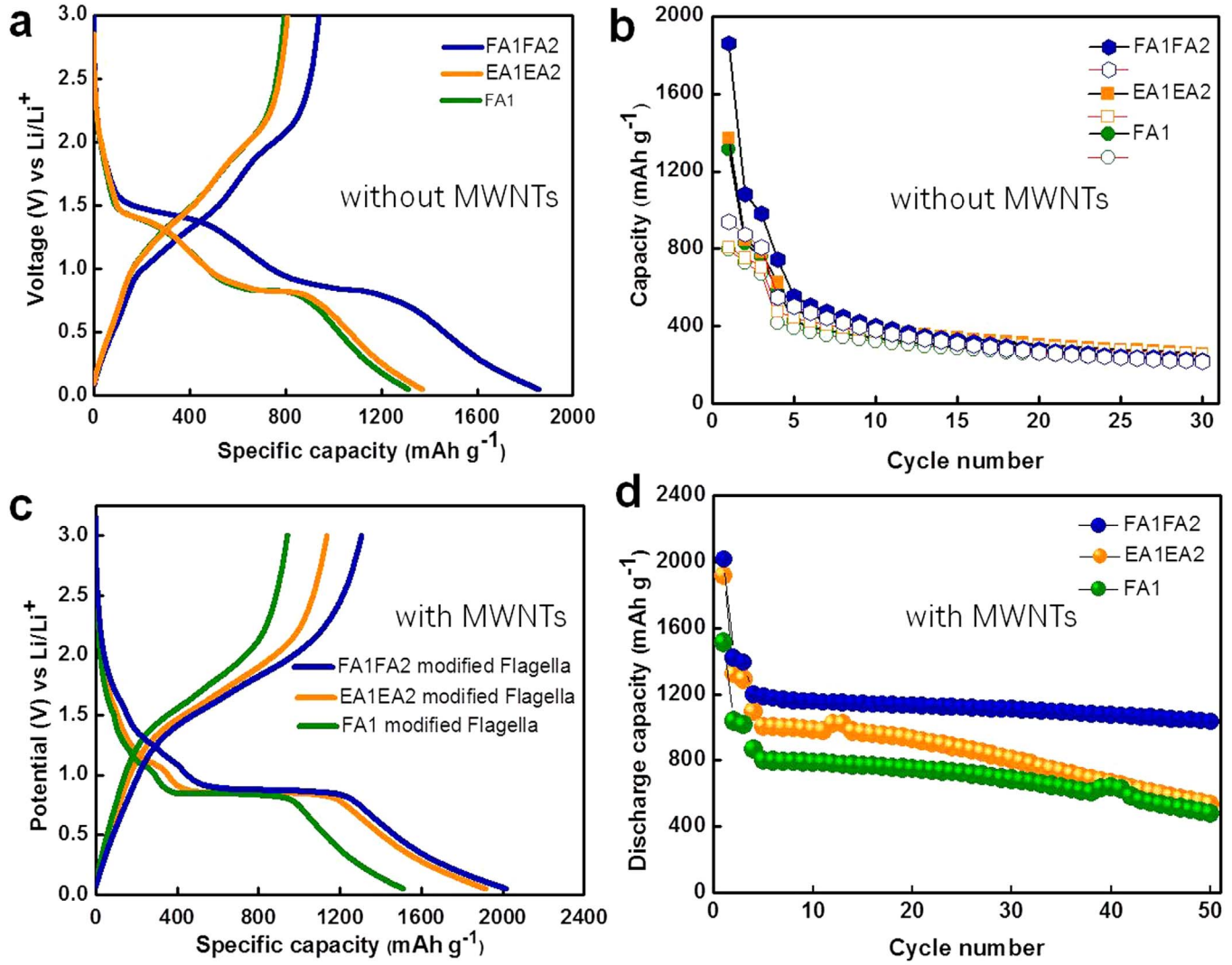

Figure 3 | Voltage profiles and electrochemical cycling with Lithium (a), (c) First charge-discharge profiles and (b), (d) cycling behavior of mineralized Fe_2O_3 samples with various peptide modifications without and with MWCNTs, resectively.

performance of the composite materials in this case. The experimentally observed better properties of FA1FA2 sample may be due to higher density of mineralized iron oxide around the flagella scaffold, which implies more effective binding Fe^{3+} ions with inserted tetra-aspartate, and it certainly requires further investigations. To further probe the effect of MWCNTs content on the electrochemical performance, we have made a series of composites. To test the power capability of the samples, high current rates from 500 mA g^{-1} to 5 A g^{-1} were applied to the electrode. Figure 4a represents the discharge profiles of the mineralized Fe_2O_3 samples with 10% MWCNTs loading at various current rates. Though cycling performance of FA1FA2 sample is superior to FA1 and EA1EA2 samples at 593 mA g^{-1}, the EA1EA2 modified flagella samples show slightly better power capability at very high current rates (Fig. 4b). The inset of Fig. 4b shows the Ragone plot for the three different peptide modifications, which again illustrates the high specific energy (Wh kg^{-1}) of the EA1EA2 sample at high specific powers (W/kg). The reversible discharge capacity was as high as 770 mAh g^{-1} with the EA1EA2 sample at 5 A g^{-1}. There are very few reports available in the literature demonstrating high rate performance of biologically synthesized negative electrodes[5,10,31]. The rate performance suggests that FA1FA2 and EA1EA2 samples are high rate capable and show promising reversible capacity of 993 mAh g^{-1} after 40 cycles.

To probe the effect of MWCNTs loading, the power performance of the FA1FA2 sample is depicted in Fig. 4c. The performance improves with increasing MWCNT content such that at 5 A g^{-1} the composite materials were able to deliver 950 mAh g^{-1} with 15 weight % loading of MWCNTs (Fig. 4c). The corresponding electrical resistivity values are shown in the supplementary information (Fig. S4 and Table S3) for different peptide modifications with varying MWCNT loadings. The reason behind the superior performance of the FA1FA2 modified flagella compared to other samples is not clearly understood at this stage and further studies are essential to understand the lithium storage reaction mechanism. As control experiments, mineralized Fe_2O_3 samples synthesized without any modifications on the flagella and without any flagella, were also tested. The results show continuous capacity degradation from 800 to 400 mAh g^{-1} for both samples (shown as supplementary, Fig. S5).

We have also carried out morphological analysis of FA1FA2-Fe_2O_3 electrodes before and after cycling. FE-SEM images were taken before and after 5th, 10th and 30th cycles. Figure S6 confirms the morphology retention of FA1FA2-Fe_2O_3 samples after continuous cycling. This further confirms that the functional materials synthesis using nanobiotechnology offers morphological stabilization of the active materials during electrochemical reaction and suppresses the agglomeration of active materials.

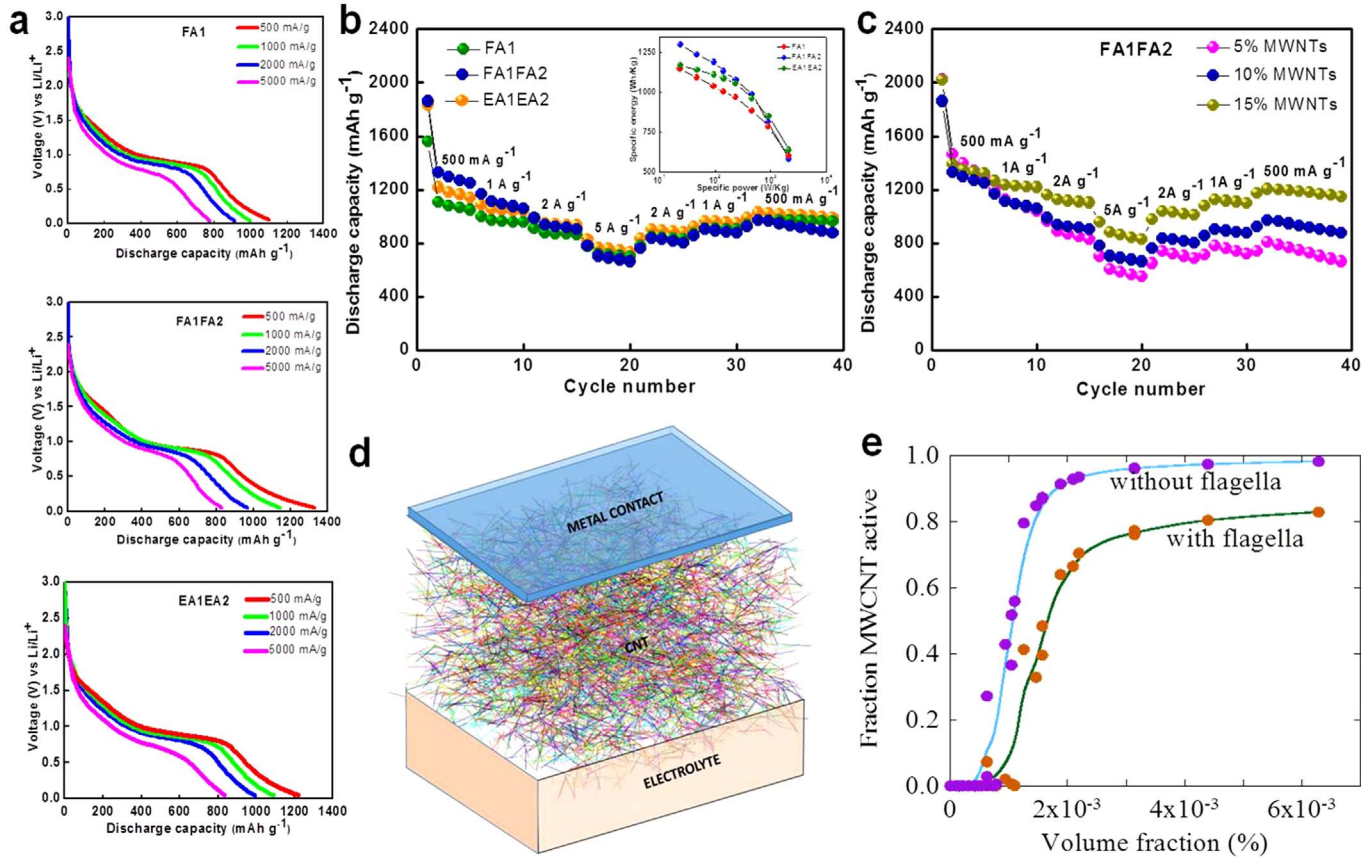

Figure 4 | Voltage profiles at various rates, rate capability and Monte Carlo simulation (a) Discharge profiles and (b) rate performance of mineralized Fe_2O_3 samples with various peptide modifications with 10% MWCNTs. Inset of b shows Ragone plot of the same electrode, (c) rate performance of FA1FA2 mineralized by Fe_2O_3 sample with various MWCNTs loading (5, 10 and 15 weight %), (d) A simulation study on MWCNT network formation between current collector (metal) contact and electrolyte and (e) Fraction of active MWCNTs in the network with and without flagella.

To decipher the percolation phenomena of the MWCNTs in the flagella samples mineralized with Fe_2O_3, a Monte Carlo study of electrical and ionic percolation in bundles of MWCNTs was carried out (details are given in methods section and supplementary information, Fig. S7). In a typical simulation, MWCNT bundles are randomly introduced into a box of a fixed volume. Pairs of nearest-neighbour bundles are chosen randomly and are allowed to form connections with each other as a result of short-range attractive interactions between the nanotube bundles. A conducting path is realized in the 3-D network when the volume fraction of the nanotube bundles exceeds the percolation threshold of $1.01x10^{-3}$% vol. where 50% of the MWCNTs can simultaneously conduct electrons and ions (Fig. 4d).The introduction of flagellar filaments into the MWCNT network results in a change in percolation threshold. Different volume fractions of MWCNT-flagella composites are studied with flagella comprising 10 weight % of the composite material. Figure 4e, shows the change in the percolation threshold to $1.7x10^{-3}$% vol. of the composite material as loading is modified. The introduction of flagella also results in a slight increase in the fraction of the MWCNTs being electrochemically inactive.

To summarize, this report describes the use of archaeal flagella biotemplates that are more environmental and human friendly for the synthesis of metal oxide (Fe_2O_3) nanostructures. These template materials can exhibit superior power and rate performance compared to existing literature to date. This approach to active oxide materials synthesis has potential across a range of applications from battery materials to other forms of electro-catalysts for important energy applications.

Methods

Development of *H. salinarum* strains producing the modified flagellins. The strains were obtained by the transformation of *H. salinarum* cells with appropriate plasmids (Table S1) using polyethylene glycol (PEG) as previously described elsewhere[32]. The selection of transformants was carried out on agar medium containing 15% sucrose and 0.1–0.2 μg mL^{-1} novobiocin (Sigma, USA). Since all plasmids used in the work do not contain the archaeal replication origin, the antibiotic resistance is acquired only after the plasmid insertion into the chromosome by the mechanism of homologous recombination. Incubation was carried out at 37°C for 10–14 days. Modified *H. salinarum* genomes contained both the modified and native flagellin *flgA* operon. Modified *H. salinarum* cells were stored on 1.5% agar plates with the appropriate media at room temperature.

Flagella isolation. Flagella isolation was performed as described earlier[21]. Briefly, *H. salinarum* cells were cultured in 1 L flasks with 200 mL of medium until the late plateau phase. The resulting biomass was pelleted by centrifugation at 8000 g for 30 min. The supernatant was treated with 4% PEG-6000, and then the flagella were precipitated by centrifugation at 15000 g for 45 min. Additionally, the flagella were purified by centrifugation in CsCl density gradient (12 h at 55000 rpm, VTi-80 rotor, Beckman, USA). Cesium chloride was dissolved in a saline medium upto the final density of 1.36 g cm^{-3}. The presence of flagella helps in the formation of a visible zone in the middle of the tube. The fraction was diluted (10-fold) with saline medium containing 25% NaCl and 20 mM Mg_2SO_4, and then the flagella were pelleted by centrifugation at 80000 g for 1 h.

Iron oxide binding and composite formation with MWCNTs. Before mineralization the isolated flagella were sonicated at 44 KHz frequency using an UZDN ultrasonic disperser (Selmi, Ukraine) on ice water bath. Sonication was continued for 40 min in periods of 1 min, with pauses of 1 min to cool the treated sample. Sonicated flagella were exposed in water solution containing 0.15 M NaCl and 18 mM iron (III) chloride at concentration of 0.1 mg mL^{-1} for 1 h at 20°C. Then, 3 M $NaBH_4$ solution was added drop wise to the reaction mixture to final concentration of 100 mM. Precipitate of Fe_2O_3 mineralized flagella was washed twice by water and then by 70% ethanol in water. The mineralized flagella were dried for 12 h at 60°C and used for electrode fabrication. To fabricate composite, required amount of MWCNTs (5, 10 or 15 weight %) were dispersed in mixed solvent of water and acetonitrile using ultra sonication. Flagella mineralized with Fe_2O_3 were added to the MWCNTs dispersion with the aid of sonication. The resulting dispersion was heated at 80°C for 3 h with the addition of hydrazine. The resulting solution was washed with acetone and dried in vacuum at 60°C for 12 h to obtain MWCNTs/

Fe_2O_3-flagella composite. The dried samples were used for electrode fabrication for electrochemical measurements.

Electrochemical characterization. Negative electrodes were prepared by mixing MWCNTs/Fe_2O_3-flagella composite (80 wt. %) with 10 wt.% super C-65 prior to slurry making. PVDF (10 wt.%) was dissolved in N-methyl pyrrolidone (NMP) and the pre-mixed mixture was dispersed in the binder solution using ultrasonication followed by continuous stirring to form homogeneous slurry. The slurry was tape cast on Cu foil using doctor blade technique. The foils were dried in vacuum at 100°C for 12 h before cell fabrication. Swagelok cells were made for electrochemical characterization using LP 30 [1 M $LiPF_6$ in 1 : 1 (weight %)] (Merck) dissolved in EC : DMC) as electrolyte, borosilicate glass fibre (GF/D, whatman) as separator, and lithium foil as reference and counter electrode. All the electrochemical tests were conducted in Arbin instruments (USA) within the potential window of 0.05–3 V at 20°C ± 1°C.

Monte Carlo study. The CNTs attract each other via short van der Waals' interactions. These interactions result in aggregation of the CNTs into a cluster. The exact form of the interactions, which are needed to accurately form the shape and size of the aggregates, are not known to us. Consequently, we develop aggregation models that qualitatively describe the observed behaviour in the experiments. CNTs are assumed to be perfectly straight and of length 1 μm. The formation of aggregated cluster from an initial random arrangement is studied using a dynamical aggregation model. The chosen number of CNTs denoted as N are initially placed randomly in a box of dimensions L_x, L_y and L_z in the x-, y- and z-directions, respectively. Two CNTs are said to be in contact when the spacing between them is less than 1 nm. Initially, few of the CNTs might be in contact. Subsequently, we perform Monte Carlo steps where a CNT is randomly chosen. When the CNT does not have any contact, the position of CNT center of mass undergoes a translation operation and a contact is formed with the nearest CNT. Such a step is shown in Fig. S7a (as supplementary information). The CNT orientation is rotated about the point of contact when a single contact has already been formed with another CNT. The rotation operation is made such that the CNT forms contact with a second CNT, such that now it has two contacts. Such a step is shown in Fig. S7b (as supplementary information). Suppose no CNT is found nearby which will result in the formation of a second contact, the CNT will contain only a single contact point in the entire simulation. These steps are performed 100 N times to obtain the final aggregated structure.

The top 1 μm of the box is assumed to be electronically conducting; any CNT in this region is said to be electronically-active as it can conduct electrons. CNTs in contact with such CNTs are also electronically-active. Similarly, the bottom 1 μm of the box is assumed to be ionically conducting; any CNT in this region is said to be ionically-active as it can conduct ions. CNTs that are both electronically- and ionically-active are electrochemically active as the reduction (oxidation) of Li^+ (Li) is possible. Presence of electrochemically-active CNTs is sought. The nature of aggregation depends on the number of CNTs and the height of the box. The aggregated CNTs often do not form percolating networks that connect the electronically-active region to the ionically-active region. The thickness of a nanobundle can increase with time due to agglomeration, which results in a concomitant decrease in the volume fraction of the nanobundles. The effect of aggregation is studied by considering different volume fractions of CNTs. Since timescales of agglomeration dynamics are generally slow, it is expected that the volume fraction of the nanotube bundles will decrease gradually over time resulting in a decrease in the fraction of electrochemically active bundles.

1. Aricò, A. S., Bruce, P., Scrosati, B., Tarascon, J.-M. & Schalkwijk, W. V. Nanostructured materials for advanced energy conversion and storage devices. *Nat. Mater.* **4**, 366–377 (2005).
2. Bruce, P. G., Scrosati, B. & Tarascon, J.-M. Nanomaterials for rechargeable lithium batteries. *Angew. Chem. Int. Ed.* **47**, 2930–2946 (2008).
3. Sanchez, C., Arribart, H. & Guille, M. M. G. Biomimetism and bioinspiration as tools for the design of innovative materials and systems. *Nat. Mater.* **4**, 277–288 (2005).
4. Sanghamitra, N. J., Inaba, H., Kitagawa, S. & Ueno, T. Inorganic design of protein assemblies as supramolecular platforms. *J. Inorg. Organomet.* **23**, 50–60 (2013).
5. Nam, K. T. *et al.* Virus-enabled synthesis and assembly of nanowires for lithium ion battery electrodes. *Science* **312**, 885–888 (2006).
6. Lee, Y. J. *et al.* Fabricating genetically engineered high-power lithium-ion batteries using multiple virus genes. *Science* **324**, 1051–1055 (2009).
7. Oh, D. *et al.* Biologically enhanced cathode design for improved capacity and cycle life for lithium-oxygen batteries. *Nat. Commun.* **4**, 2756 (2013).
8. Peled, E., Golodnitsky, D. & Penciner, J. Handbook of Battery Materials Besenhard, J. O. Ed. pp 648 (Wiley-VCH, Weinheim, Germany, 1999).
9. Poizot, P., Laruelle, S., Grugeon, S., Dupont, L. & Tarascon, J.-M. Nano-sized transition metal oxides as negative electrode material for lithium-ion batteries. *Nature* **407**, 496–499 (2000).
10. Miot, J. *et al.* Biomineralized α-Fe_2O_3: texture and electrochemical reaction with Li. *Energy Environ. Sci.* **7**, 451–460 (2014).
11. Cabana, J., Monconduit, L., Larcher, D. & Palacin, M. R. Beyond Intercalation-Based Li-Ion Batteries: The State of the Art and Challenges of Electrode Materials Reacting Through Conversion Reactions. *Adv. Mater.* **22**, E170–E192 (2010).
12. Larcher, D. *et al.* Combined XRD, EXAFS, and Mössbauer studies of the reduction by lithium of α Fe_2O_3 with various particle sizes. *J. Electrochem. Soc.* **150**, A1643–A1650 (2003).
13. Sun, Y., Zhang, J., Huang, T., Liu, Z. & Yu, A. Fe_2O_3/CNTs composites as anode materials for lithium-ion batteries. *Int. J. Electrochem. Sci.* **8**, 2918–2931 (2013).
14. Ban, C. *et al.* Nanostructured Fe_3O_4/SWNT Electrode: binder free and high rate Li-ion anode. *Adv. Mater.* **22**, E145–E149 (2010).
15. Wang, J. Z. *et al.* Graphene encapsulated Fe_3O_4 nanoparticles with 3D laminated structure as superior anode in lithium ion batteries. *Chem.-Eur. J.* **17**, 661–667 (2011).
16. Dong, W. & Zhu, C. Use of ethylene oxide in the sol–gel synthesis of α-Fe_2O_3 nanoparticles from Fe (III) salts. *J. Mater. Chem.* **12**, 1676–1683 (2002).
17. Taberna, P. L., Mitra, S., Poizot, P., Simon, P. & Tarascon, J.-M. High rate capabilities Fe_3O_4-based Cu nano-architectured electrodes for lithium-ion battery applications. *Nat. Mater.* **5**, 567–573 (2006).
18. Chou, S. L. *et al.* High-surface-area α-Fe_2O_3/carbon nanocomposite: one-step synthesis and its highly reversible and enhanced high-rate lithium storage properties. *J. Mater. Chem.* **20**, 2092–2098 (2010).
19. Kumara, M. T., Srividya, N., Muralidharan, S. & Tripp, B. C. Bioengineered flagella protein nanotubes with cysteine loops: Self-assembly and manipulation in an optical trap. *NanoLett.* **6**, 2121–2129 (2006).
20. Wang, F., Li, D. & Mao, C. Genetically modifiable flagella as templates for silica fibers: from hybrid nanotubes to 1D periodic nanohole arrays. *Adv. Funct. Mater.* **18**, 4007–4013 (2008).
21. Beznosov, S. N., Pyatibratov, M. G. & Fedorov, O. V. Archaeal flagella as matrices for new nanomaterials. *Nanotechnol. Russ.* **4**, 373–378 (2009).
22. Beznosov, S. N., Pyatibratov, M. G., Fedorov, O. V., Kulova, T. L. & Skundin, A. M. Electrochemical properties of nanostructured material based on modified flagella of halophilic archaea *Halobacterium salinarum* for negative electrode of lithium-ion battery. *Nanotechnol. Russ.* **6**, 705–710 (2011).
23. Jo, W., Freedman, K. J., Yi, D. K. & Kim, M. J. Fabrication of tunable silica-mineralized nanotubes using flagella as bio-templates. *Nanotechnology* **23**, 055601 (2012).
24. Schiraldi, C., Giuliano, M. & Rosa, M.-D. Perspectives on biotechnological applications of archaea. *Archaea* **1**, 75–86 (2002).
25. Jarrell, K. F., Ding, Y., Nair, D. B. & Siu, S. Surface appendages of Archaea: structure, function, genetics and assembly. *Life* **3**, 86–117 (2013).
26. Beznosov, S. N., Pyatibratov, M. G., Veluri, P. S., Mitra, S. & Fedorov, O. V. A way to identify archaellins in *Halobacterium salinarum* archaella by FLAG-tagging. *Cent. Eur. J. Biol.* **8**, 828–834 (2013).
27. Tarasov, V. Y., Pyatibratov, M. G., Tang, S. L., Dyall-Smith, M. & Fedorov, O. V. Role of flagellins from A and B loci in flagella formation of *Halobacterium salinarum*. *Mol. Microbiol.* **35**, 69–78 (2000).
28. Hopp, T. P. *et al.* A Short Polypeptide Marker Sequence Useful for Recombinant Protein Identification and Purification. *Biotechnology* **6**, 1204–1210 (1988).
29. Malachowski, L. & Holcombe, J. A. Comparison of immobilized poly-L-aspartic acid and poly-l-glutamic acid for chelation of metal cations. *Anal. Chim. Acta* **517**, 187–193 (2004).
30. Buchan, D. W. A., Minneci, F., Nugent, T. C. O., Bryson, K. & Jones, D. T. Scalable web services for the PSIPRED protein analysis workbench. *Nucl. Acids Res.* **41**, W349–W357 (2013).
31. Rosant, C. *et al.* Biosynthesis of Co_3O_4 electrode materials by peptide and phage engineering: comprehension and future. *Energy Environ. Sci.* **5**, 9936–9943 (2012).
32. Cline, S. W., Lam, W. L., Charlebois, R. L., Schalkwyk, L. C. & Doolittle, W. F. Transformation methods for halophilic archaebacteria, *Can. J. Microbiol.* **35**, 148–152 (1989).

Acknowledgments

The authors acknowledge the financial support by the Russian Foundation for Basic Research, project No.12-04-92691_IND_a, and Department of Science and Technology, Government of India, project code INT/RFBR/P-126. The authors are deeply grateful to NCPRE-MNRE and Indian Institute of Technology Bombay for instrumental and infrastructure supports.

Author contributions

S.N.B. carried out the synthesis, and P.S.V. designed and conducted the electrochemical experiments. M.G.P., O.V.F., D.R.M. and S. M. designed the research approach and suggested the experiments. P.S.V. carried out the TEM and SEM studies; A.C. and S.M. developed the theoretical framework and A.C. derived the model and conducted the simulations; M.G.P., D.R.M. and S.M. wrote the manuscript and all authors discussed the experiments to draft the final manuscript.

Additional information

Supplementary information accompanies this paper at http://www.nature.com/scientificreports

Competing financial interests: The authors declare no competing financial interests.

How to cite this article: Beznosov, S.N. *et al.* Flagellar filament bio-templated inorganic

oxide materials – towards an efficient lithium battery anode. *Sci. Rep.* **5**, 7736; DOI:10.1038/srep07736 (2015).